

Diffusion of 1,2-Dimethoxyethane and 1,2-Dimethoxypropane through Phosphatidylcholine Bilayers: A Molecular Dynamics Study

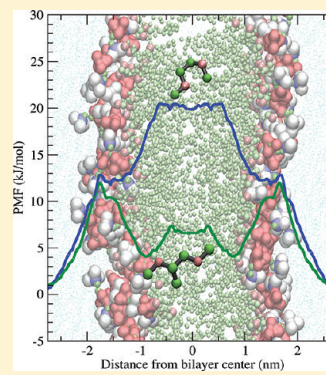
Susruta Samanta,[†] Samira Hezaveh,[†] Giuseppe Milano,[‡] and Danilo Roccatano*,[†]

[†]School of Engineering and Science, Jacobs University Bremen, Campus Ring 1, D-28759 Bremen, Germany

[‡]Department of Chemistry, University of Salerno, I-84084 Fisciano (Salerno), Italy

Supporting Information

ABSTRACT: In this paper, a theoretical study of 1,2-dimethoxyethane (DME) and 1,2-dimethoxypropane (DMP) at water/*n*-heptane and 1,2-dimyristoyl-*sn*-glycero-3-phosphatidylcholine (DMPC) lipid bilayer/water interfaces using the umbrella sampling method is reported. Recently proposed GROMOS96/OPLS compatible models for DME and DMP have been used for the simulation studies. The percolation free energy barrier of one DME and DMP molecule from water to *n*-heptane phase calculated using the umbrella sampling method turned out to be equal to ~ 18.5 kJ/mol and ~ 6 kJ/mol, respectively. In the case of the DMPC lipid bilayer, overall free energy barriers of ~ 20 kJ/mol and ~ 12 kJ/mol were obtained for DME and DMP, respectively. The spontaneous diffusion of DME and DMP in the lipid bilayer has also been investigated using unconstrained molecular dynamics simulations at the water/DMPC interface and inside the lipid bilayer. As expected from the estimated percolation barriers, simulation results show that DME, contrary to DMP, spontaneously diffuse into the aqueous solution from the lipid interior. In addition, simulations with multiple DME or DMP molecules at the interface show spontaneous diffusion within 50 ns inside the DMPC layer only for DMP.



INTRODUCTION

Ether-based molecules such as crown-ethers, polymers, and especially polyethylene oxide (PEO)- and polypropylene oxide (PPO)-based copolymers are of great interest for basic research and also for their applications in biotechnology and medicine.^{1–6} A significant amount of work has been published on the applications of block copolymers in the medical and pharmaceutical fields.⁷ In fact, block copolymers, being inexpensive, nontoxic, and easily available, are promising substitutes for lipopolymers for drug delivery.⁸ As an example, encapsulation in polymer of peptide-based drugs increases residence time and bioavailability by decreasing the chances of proteolytic decomposition.^{2,3,5,6,9,10} Other interesting applications include, for example, the use of crown ether-modified peptide to create artificial membranes or grafting of lipids and polymers to achieve specific bioactivities.^{11–14}

For all these applications, it is of utmost importance to understand the atomistic details of the interaction of these molecules with biological membranes. Although a good number of experimental studies have already been done on the structural characteristics and interactions of ethylene oxide/propylene oxide-based polymers with biomembranes and lipid bilayers,^{10,15–17} the details of permeation of these polymers systems across lipid membrane itself are not well-known at the molecular level. Therefore, atomistic simulations of these polymers at the interface of lipid bilayers can shed light on these processes. The simplest models of these polymers are the 1,2-dimethoxyethane (DME) and 1,2-dimethoxypropane (DMP) molecules (Figure 1). They can be considered as the

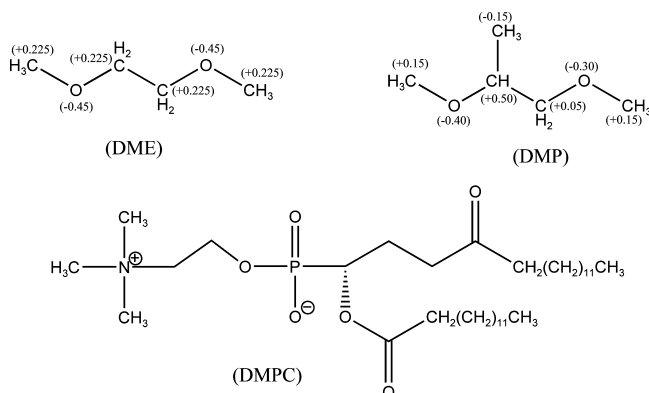


Figure 1. Molecular structures of DME, DMP, and one chain of DMPC. Partial charge on the heavy-atoms of the DME and DMP molecules are shown in parentheses.

smallest oligomers of the PEO and PPO polymers, the building blocks of common biocompatible block copolymers. Despite the widespread biomedical applications of these molecules, accurate molecular dynamics (MD) simulations studies to assess their thermodynamics and dynamics of the interaction with biological interfaces are limited.^{18–23} One of the reasons for so few studies is the time scale of this process, which can go

Received: December 1, 2011

Revised: March 1, 2012

Published: March 12, 2012

beyond the capacity of standard MD simulations. A more convenient way to simulate these processes is the use of potential driven and/or constrained MD simulations. The steered molecular dynamics (SMD) method^{24,25} (also known as “pulling simulation”) is commonly used to drive a process along a given pathway by applying an external constant force to the system. The additional force allows the system to easily overcome energy barriers speeding up the simulation of the process.^{18,26,27} The integration along the pathway of the variation of this external force provides the potential of mean force (PMF) of the process. SMD, being a nonequilibrium method, requires a large number of pulling simulations to provide a reliable PMF profile from which one can derive thermodynamic properties with good accuracy.^{25,28,29} An equivalent approach to the SMD is the umbrella sampling (US) method.³⁰ In this case, the PMF properties of the system are obtained by conformational sampling along the reaction pathway (generated, for example, by an SMD simulation) to generate overlapped probability distributions. The resulting distributions are then combined with the weighted histogram analysis method (WHAM) to reconstruct the barrier.³¹ These two techniques have been used to study small molecules^{32–35} and polymer^{18,36} permeation in lipid bilayers with good accuracy. Nevertheless, to the best of our knowledge, a quantitatively accurate characterization of the lipid bilayer permeation barrier by DME and DMP molecules has not yet been performed. In the present work, we use the recently published force field models for DME and DMP molecules³⁷ to study their interaction with *n*-heptane and 1,2-dimyristoyl-sn-glycero-3-phosphatidylcholine (DMPC) lipid bilayer interfaces and characterize, using both SMD and US methods, the percolation barriers through them. The models of DME and DMP are further validated by calculating their partition coefficient between 1-octanol and water. The percolation of DME and DMP through water/*n*-heptane interface was investigated to understand their behavior in the presence of a simple hydrophobic interface, which is comparable to the aliphatic tail region of the lipid bilayer.

The paper is organized as follows: The details of force fields and simulation procedures are given in the Methods section. In the first part of the Results and Discussion, the results obtained from US simulations of percolation of both DME and DMP through *n*-heptane/water and DMPC/water interfaces are reported. In the second part, free simulations of DME and DMP at the DMPC interface are performed to investigate the occurrence of a spontaneous diffusion process. Finally, in the Conclusions section, a summary of the properties of DME and DMP at interfaces and the implications for the interaction of a polymer with a biological membrane are summarized.

METHODS

Force Field. For the DMPC bilayer, the united atom model of Berger et al.³⁸ was used. This lipid model is a combination of GROMOS and OPLS parameters, optimized to reproduce the experimental physical properties of a lipid bilayer. For DME and DMP, the recent models by Hezaveh et al.³⁷ were used. For the water model, the simple point charge (SPC)³⁹ model was used, and for 1-octanol and *n*-heptane, the OPLS united atom (OPLS-UA) model^{40,41} was used.

Simulation Setup. All the simulations were performed using the GROMACS (version 4.0.7)⁴² software package. The program VMD⁴³ was used for the graphical representation of the molecular systems.

For the water/*n*-heptane interface system, 208 *n*-heptane molecules were sandwiched between ~3350 water molecules along the *z*-direction in a box of dimensions $3.7 \times 3.7 \times 11.2 \text{ nm}^3$. The lipid bilayer simulations were performed using a simulation box containing one DME or DMP molecule and a bilayer composed of 128 DMPC lipids chains, 64 for each layer. The box had dimensions of $6.4 \times 6.4 \times 9.5 \text{ nm}^3$, and it was filled with ~8000 water molecules for a total of ~30 000 atoms. A schematic diagram of the position and density distribution of the DMPC bilayer along with the relevant components of the system is shown in Figure 2.

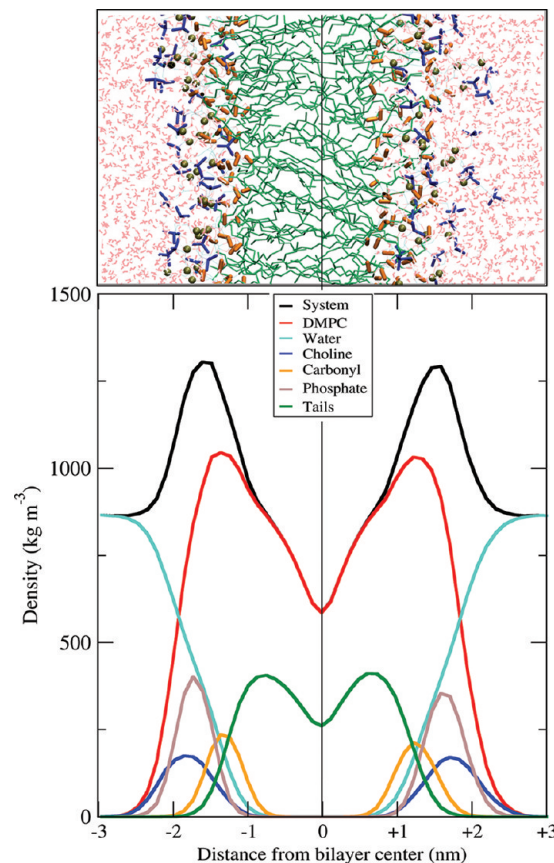


Figure 2. Schematic diagram of the density profile of the DMPC bilayer along the *z*-axis. A snapshot of the simulated system is shown above. For better understanding of the position of the components, they are shown in different colors: water molecules in red, the choline groups in blue, the carboxylic groups in orange, the phosphate groups as tan spheres, and the aliphatic chains are shown in green. The density profile of the whole system along with relevant components of the system are shown in the bottom half.

The bilayer simulations were performed at 310 K, above the crystalline fluid/liquid phase transition temperature, using the V-rescale thermostat⁴⁴ with a coupling constant of 0.1 ps. For comparison, the temperature of the water/*n*-heptane systems was set the same. The pressure was kept constant at 1 bar using a Berendsen barostat⁴⁵ with a coupling constant of 0.5 ps. For lipid bilayer simulations, a semi-isotropic barostat was used to take in account the difference in compressibility of the system along the *x*, *y*, and *z* directions. The bond lengths were constrained using the LINCS⁴⁶ algorithm. An integration time step of 2 fs was used for all the simulations. Electrostatic interactions were evaluated using particle mesh Ewald

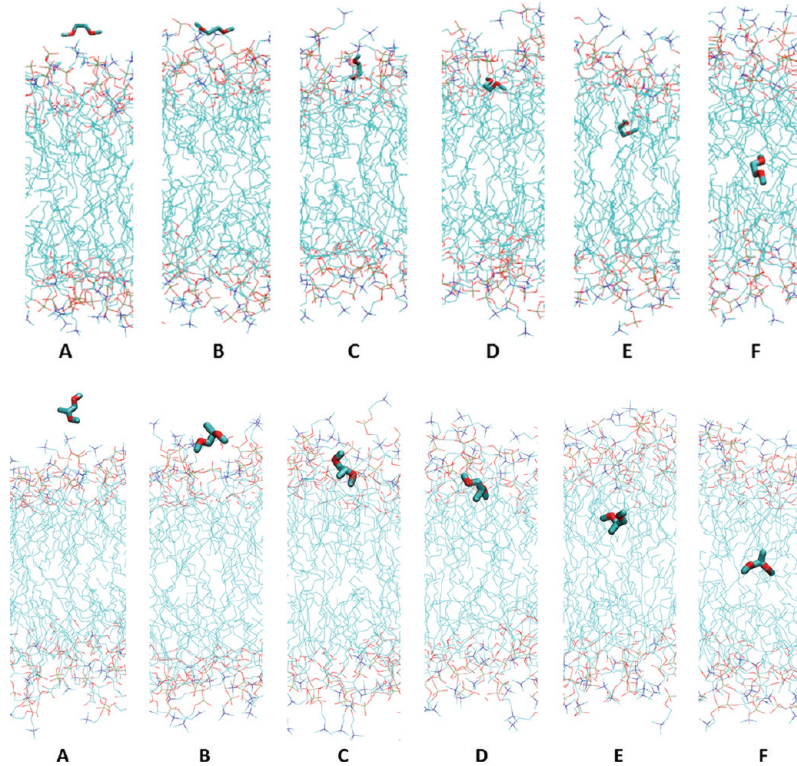


Figure 3. The selected six frames from the US simulations for detailed investigations. These specific frames were used as the starting configuration for unconstrained simulations. Initial positions of DME with respect to the bilayer are shown in the top row, and that for DMP is shown in the bottom row.

method⁴⁷ with a cutoff of 1.0 nm, grid spacing of 0.12 nm, and a fourth order spline interpolation. Lennard-Jones interactions were truncated at 1.0 nm.

Calculation of the Free Energy of Solvation and Partition Coefficient. Simulations were performed in 1-octanol as a solvent for calculating the partition free energy of DME and DMP in water/1-octanol. One molecule of DME or DMP was centered in a ~4 nm/side cubic box including 124 1-octanol molecules. Gibbs free energy of solvation in 1-octanol (ΔG_{sol}) at 298 K was calculated for both molecules using the thermodynamic integration (TI) method.⁴⁸ The Gibbs free energy of solvation in water (ΔG_{hyd}) and in vacuum (ΔG_{vac}) were taken from our recent publication.³⁷ The TI integration was performed on 17 λ points: 0, 0.01, 0.05, 0.1, 0.2, 0.3, 0.4, 0.5, 0.55, 0.6, 0.65, 0.7, 0.8, 0.9, 0.95, 0.98, and 1.00. The λ points were chosen in order to get a smooth variation of the $dH/d\lambda$ curve. The soft-core parameters α and σ were assigned the values of 1.51 and 0.30 respectively, as suggested by Villa and Mark.⁴⁹ For each λ , the system was first equilibrated for 150 ps followed by a production run of 500 ps. The ΔG_{vac} was subtracted from the ΔG_{oct} value in 1-octanol to obtain the final ΔG_{sol} value. From ΔG_{sol} and ΔG_{hyd} at the temperature T , the corresponding partition coefficient was calculated according to the following formula:⁴¹

$$\log P_{\text{1-octanol/water}} = \frac{\Delta G_{\text{hyd}} - \Delta G_{\text{sol}}}{2.303RT} \quad (1)$$

where R is the universal gas constant.

SMD Simulations. The SMD method was used to speed up the diffusion of DME/DMP through (a) the *n*-heptane layer and (b) one of the monolayers of the DMPC bilayer. The SMD simulations were performed to obtain the frames for US

simulations and also to test the convergence of the two methods. The SMD simulations were performed using a slow pulling regime to ensure operation in near-equilibrium conditions.²⁹ The pulling parameters adopted by Pal et al.¹⁸ to study the percolation of a PEO chain through a DMPC lipid bilayer were used. For qualitative estimations, SMD takes less computational time and resources than the US methods. However, being a nonequilibrium method, the calculation of the equilibrium properties require multiple number of pulling trajectories to obtain a reliable sampling.^{25,29} From the initial tests (details in Figures S1 and S2 in the Supporting Information (SI)), it was clear that it is not possible to rely on a relatively small number of SMD simulations for the calculation of quantitative free energy profile for a complex system like this. Therefore, the SMD simulations were mainly used to generate starting points for the US simulations.

US Simulations. The US method was used to calculate the free energy profiles for the percolation of the DME and DMP molecules through *n*-heptane and DMPC layer. This method has been recently used by MacCallum et al.³² to study the diffusion of small amino acid side chain model molecules through lipid bilayers. In the present work, we have adopted a similar procedure. A harmonic restraint with a force constant 3000 kJ/mol nm² was applied to the distance between the center of mass (CoM) of the DME/DMP molecule and the head groups of the bottom DMPC layer, in the direction normal to the bilayer. Fifty starting US configurations of both DME and DMP molecules were taken from the path of one of the SMD trajectories. The first configuration was taken at least 3 nm away from the bilayer center, and the last one was taken in the bilayer center. The difference of distances between the CoM of the DME/DMP molecules and the reference group for

two consecutive conformations was always less than 0.1 nm to ensure the correct calculation of the PMF profile. The same method was used for the water/*n*-heptane interface system. In this case, the *n*-heptane molecules were set to be the reference group, and ~65 configurations taken from one SMD simulation were selected for US. Each frame was simulated for 5 ns. The distance was sampled at every 100 fs. The WHAM³¹ was used to calculate the PMF profile. The free energy profiles obtained from the calculations were rescaled to assign a zero reference value to the profiles in the bulk water. In the case of US, three different simulations of length 1, 5, and 7 ns were used to evaluate the convergence of the PMF of the DME molecule. For the system in consideration, the PMF profile did not change for simulation lengths larger than 5 ns (Figure S3 in the SI), and therefore we have used this time scale for all the frames of US simulations of DME and DMP for both permeation through the DMPC layer and the relatively simpler *n*-heptane/water interface.

Unconstrained Simulations at the Interface. To understand the behavior of the ether molecules at interfaces, a set of 50 ns unconstrained simulations were run with DME and DMP molecules at the water/*n*-heptane interface. The simulation boxes of dimensions $3.7 \times 3.7 \times 7.6 \text{ nm}^3$ were filled with 208 molecules of *n*-heptane and ~1700 molecules of water along with one molecule of DME/DMP. Simulations were done at 310 K in NPT conditions to be consistent with the US simulations.

The diffusive behavior of DME and DMP in different positions of the DMPC/water interface was analyzed by selecting six starting conformations from the US simulations for an unconstrained run of 50 ns at 310 K. The starting positions of DME and DMP with respect to the bilayer for the selected sets are shown in Figure 3 and in the SI (Figure S8). Two additional 50 ns simulations were also run with nine molecules of DME and DMP at the interface region of the DMPC bilayer (1 nm away from the upper boundary of DMPC).

RESULTS AND DISCUSSION

Free Energy and Partition Coefficient. Gibbs free energy values for DME and DMP in 1-octanol was calculated to be 80.3 and 63.1 kJ/mol, respectively. Their ΔG values in vacuum was calculated to be 59.8 and 38.2 kJ/mol, respectively. Hence, Gibbs free energies of solvation in 1-octanol, calculated for both DME and DMP are -20.5 ± 1.3 and -24.9 ± 1.0 kJ/mol, respectively. The value for DME is in good agreement with the estimated value of -19.1 kJ/mol.^{50,51} To the best of our knowledge, the same value for DMP is not available in the literature for a direct comparison. However, the water/1-octanol partition coefficient values ($\log P$) are available for both DME and DMP. Thus, by applying eq 1 with the values of ΔG_{sol} calculated in this work and ΔG_{hyd} available from our previous work,³⁷ values of $\log P_{\text{DME}} = 0.28$ and $\log P_{\text{DMP}} = 1.57$ were obtained. These values are close to the experimental values of 0.21 and 1.78, for DME and DMP, respectively.^{52,53}

Percolation of DME and DMP through *n*-Heptane. The middle part of the DMPC bilayer is made of aliphatic chains that can be mimicked by a layer of aliphatic liquid such as *n*-heptane.⁵⁴ Therefore, as the first part of our study, the PMF barriers for the diffusion of the two molecules from water to the organic phase were calculated and then compared with those through the lipid bilayer.

In Figure 4, the PMF profiles calculated using the US method are shown. The heights of the PMF energy barriers are

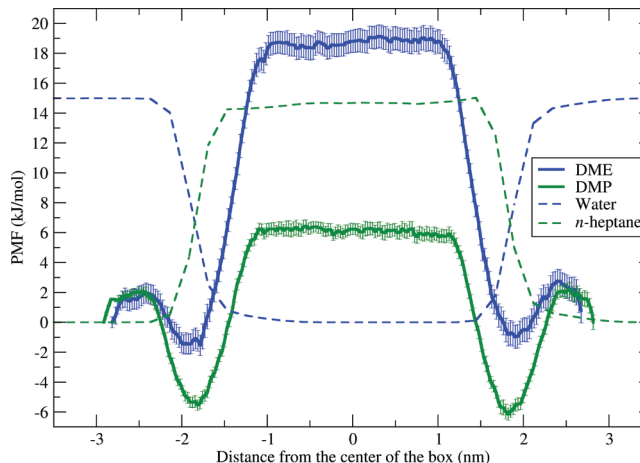


Figure 4. PMF profiles for percolation of DME (blue) and DMP (green) molecules from water to water layer through the *n*-heptane layer. The relative positions of the solvents are shown as a dashed line. The center of the box is the center of the *n*-heptane layer along the *z*-direction.

significantly different for DME and DMP, although their profiles look qualitatively similar. For DME, the height for the energy barrier (from water to *n*-heptane) is equal to ~18.5 kJ/mol, but it is only ~6.0 kJ/mol for DMP. In both profiles, minima at the *n*-heptane–water interface are observed. The origin of these minima is related to the nature of the interface. The *n*-heptane molecule, being hydrophobic, exerts repulsive force toward water, and hence molecular density drops significantly at interfaces, resulting in a reduction of the PMF in these regions.

Figure 5 (Table S1 in the SI) shows the nonbonded energy contribution of DME and DMP with other relevant components of the system, i.e., water and *n*-heptane. For this purpose, five sets of simulations from the US trajectories were considered for further analysis where the ether molecule resides in five different environments: in bulk water (1.85 nm away from the interface), in water near the interface (0.25 nm away from the interface), in the interface, in *n*-heptane near the interface (0.25 nm away from the interface) and in bulk *n*-heptane (1.85 nm away from the interface). The qualitative trend for the same potential energy components obtained from the SMD simulations along the whole pathway are reported in the SI (Figure S4). When the solutes are in the water phase, Lennard-Jones contributions with water have average values of $-61.15 (\pm 0.56)$ kJ/mol and $-73.42 (\pm 0.26)$ kJ/mol, respectively, for DME and DMP. In the *n*-heptane phase, the values of Lennard-Jones interaction energies with *n*-heptane increase to $-48.87 (\pm 0.65)$ kJ/mol and $-56.83 (\pm 0.68)$ kJ/mol, respectively, for DME and DMP. Similarly, the Coulombic energies reach minima of $-33.32 (\pm 0.57)$ kJ/mol and $-16.39 (\pm 0.43)$ kJ/mol for interaction with water for DME and DMP, respectively. As the OPLS model of *n*-heptane has null partial charges on the carbon atoms, Coulombic interactions of DME and DMP with *n*-heptane are not shown. Both of the scenarios support relatively greater affinity of DMP toward *n*-heptane than that for DME. This behavior is also evidenced in our previous study of the models.³⁷ The presence of the extra methyl group makes DMP more hydrophobic than DME and hence more soluble in aliphatic solvents.³⁷ Entering the *n*-heptane phase causes greater loss in hydrogen bonding for DME than DMP (average number of H-bonds 0.965 for DME

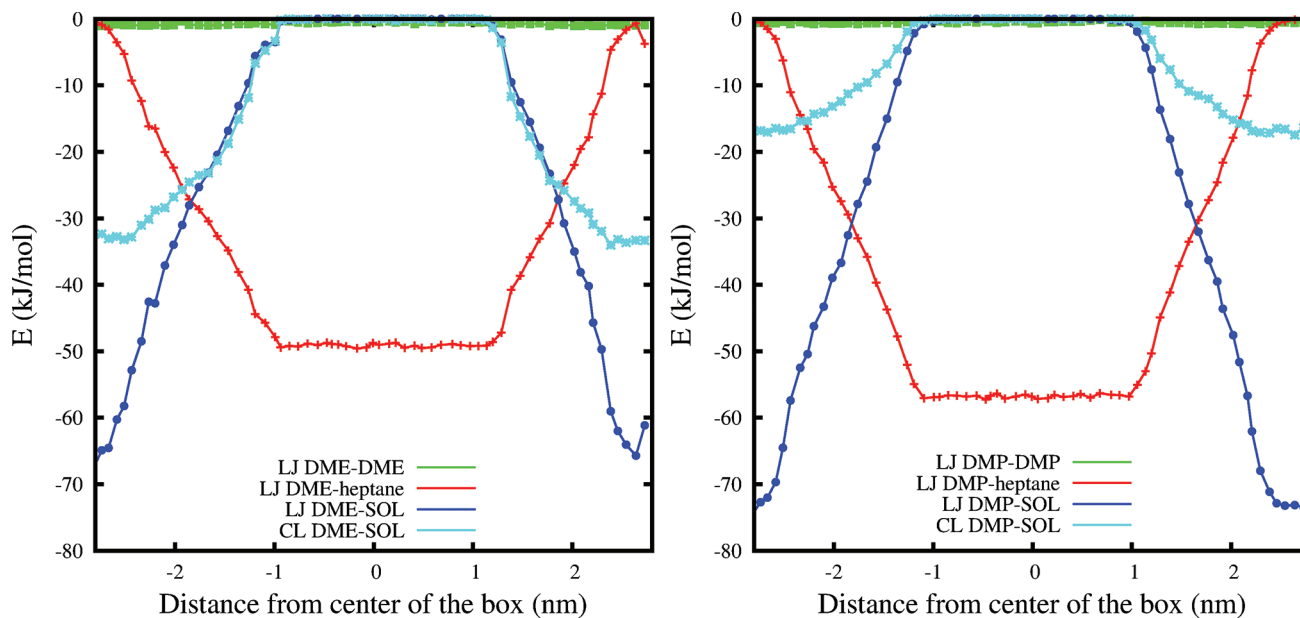


Figure 5. Nonbonded energy contribution in terms of Lennard-Jones (LJ) and Coulombic (CL) potential for percolation of DME (left) and DMP (right) through *n*-heptane. The center of the box is the center of the *n*-heptane layer along the *z*-direction.

and 0.478 for DMP), indicating a considerable reduction of the system stability. Also, the Coulombic energy contributions indicate relatively better solvation of DME in water. These factors contribute toward the upheaval of the energy barrier of percolation in the *n*-heptane phase from the water phase, resulting in a lower energy barrier for DMP than that for DME during diffusion through the *n*-heptane phase.

Simulation of DME and DMP and the Water/*n*-Heptane Interface. Figure 6 shows the density distribution

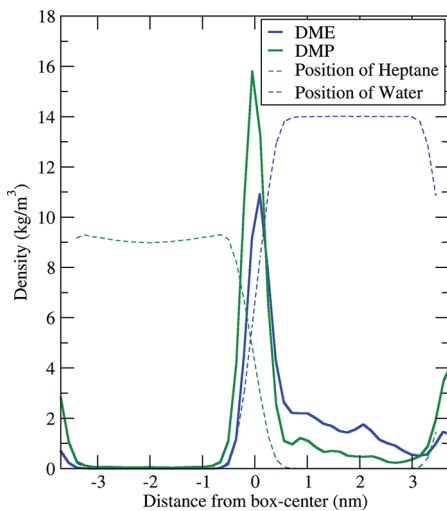


Figure 6. Average density distribution of DME and DMP during 50 ns unconstrained simulation at the water/*n*-heptane interface. The positions of the solvents are shown as a dashed line.

of DME and DMP during a 50 ns unconstrained simulation of a single ether molecule at the water/*n*-heptane interface. From the figure, it is evident that DMP has relatively higher affinity to the interface than DME. Also, the higher density of DME in the water phase indicates its higher affinity toward the water phase. Although experimental data for DME/DMP at these interfaces are not available for direct comparison, there are experimental

studies with Pluronics in air/water or air/oil interfaces.^{55–58} Since Pluronics are block copolymers having DME and DMP as their smallest oligomers, their properties at interfaces can be qualitatively compared with these systems. Neutron scattering and other techniques confirm bottle-brush type of arrangement of Pluronics at the air/oil and air/water interfaces.^{55–58} It is seen that PPO part of the polymer (of which DMP is the monomer model) accumulates at the interface region, and the PEO part (of which DME is the monomer model) flanks in the water region. Our unconstrained simulations show similar distribution of DME and DMP molecules in proximity of the *n*-heptane interface. In addition, the US simulations show the presence of a negative PMF value at the interface regions (Figure 4), and the depth of the well is greater in case of DMP (-2 kJ/mol for DME and -5.5 kJ/mol for DMP). This supports better accumulation of DMP in the interface region than DME, as seen in the experiments.

Percolation of DME and DMP through DMPC. A snapshot of the simulated system, along with partial density profiles, are shown in Figure 2. In Figure 7, the relative PMF profiles of DME and DMP are shown. For DME, the height for the energy barrier is equal to $\sim 20 \text{ kJ/mol}$, but it is only $\sim 12 \text{ kJ/mol}$ for DMP. The PMF curve of DME starts with a steep rise, and, after a small dip, the curve continues to rise smoothly until it reaches a plateau near the center of the bilayer. The initial slope in the PMF profile is obviously due to the steric effect of the bulky trimethyl amine group, which imposes an energy barrier for the process. However, as soon as the barrier is crossed, the molecule faces a relatively favorable molecular environment flanked by hydroxyl groups and ether-like oxygen atoms. Also, the density profile (Figure 2) indicates less steric hindrance in this part of the bilayer. As a result, a small dip in the PMF curve is observed. The subsequent encounter with the hydrophobic aliphatic tail region of the DMPC produces a rise in the PMF curve. After reaching the middle of the lipid bilayer, the curve converges to a plateau. In the same figure, the PMF curve for DMP is reported. As for DME, we observe an initial rise in PMF due to the steric effect of the head groups of the

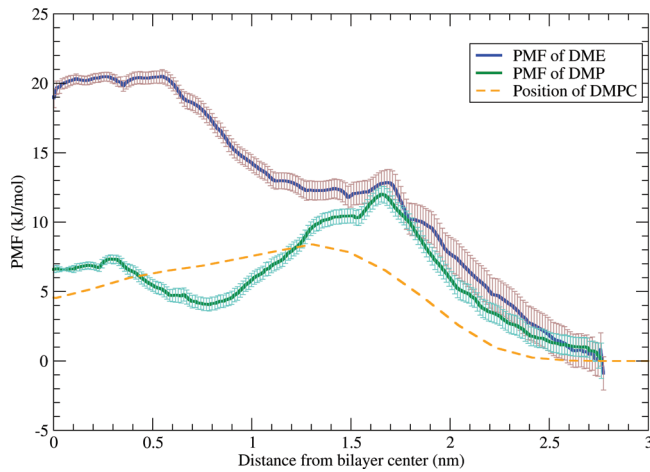


Figure 7. The comparison of PMF profiles of percolation of DME and DMP molecules using US method. The position of the DMPC bilayer is shown in orange.

DMPC upper layer, followed by a minimum due to the attraction from the next hydrophobic part of the lipid. DME having less affinity for the hydrophobic part of the lipid bilayer does not show such behavior. The relative height of the permeation barrier to the water phase is similar to that calculated for the *n*-heptane/water system. Comparing these PMF profiles with selected profiles from the work of MacCallum et al.,³² where they studied percolation of amino acid equivalent molecules (The side chains were truncated at β -carbon, and α -carbon was replaced by hydrogen. As a result, leucine, glutamine, and asparagine reduces to isobutane, acetamide and propanamide, respectively.) through a 1,2-dioleoyl-*sn*-glycero-3-phosphocholine (DOPC) bilayer, a similar trend in the qualitative and quantitative nature of the PMF profiles is observed. Although the molecules they studied are not directly comparable to the DME/DMP systems, the PMF curves for hydrophobic branched molecules (e.g., isobutane) and hydrophilic polar molecules (e.g., acetamide and

propanamide) are qualitatively similar to that of DMP and DME, respectively.

In Figure 8, average Lennard-Jones and Coulombic energies calculated for each frame of the US simulation along the pathway are shown. For a more detailed investigation, two sets of six different simulations from the US simulations for DME and DMP were considered. These simulations in the two sets are taken from distinctively different environments along the US pathways. The detailed description for nonbonded energy contributions for these sets can be found in Table S2a,b,c in the SI. The Lennard-Jones contribution for the DMPC bilayer has a minimum value of $-69.86 (\pm 0.97)$ kJ/mol for DMP, and that for DME is $-56.24 (\pm 0.48)$ kJ/mol. This indicates better stabilization of DMP in the DMPC layer. Although the Lennard-Jones contribution slightly favors DMP over DME, the comparison of Coulombic potentials of both ethers and water indicates a more favorable affinity of DME to the water phase. These factors contribute to the higher energy barrier for the percolation of DME relative to that of DMP.

The conformational population of DME molecules in the six sets of simulations was investigated. In a previous study, we showed that TGG, TGG' and TGT (where T stands for trans and G for gauche) are the three most abundant conformers of DME in aqueous and various nonaqueous (methanol, carbon tetrachloride, and *n*-heptane) solvents, and, depending on the solvent, the percent populations of the different conformers vary significantly.³⁷ In Figure 9, the histogram of the percentage values of these three conformers of DME for the six selected simulations is reported. The graph evidences a significant fluctuation in the population of the TGG (high dipole moment) and TGT (low dipole moment) conformers. The percentage of TGG conformers drops as DME enters the aliphatic region. Also, a drop in the percentage of the low dipole TGT conformers at the polar region of the bilayer is observed. These observations are also supported by our previous study of DME in different polar and nonpolar solvent systems.³⁷ In simulation C, corresponding to the DME molecule residing in the middle of the polar region of the bilayer (Figure 3), all the conformers have comparable contribution (Figure 9). This indicates large conformational

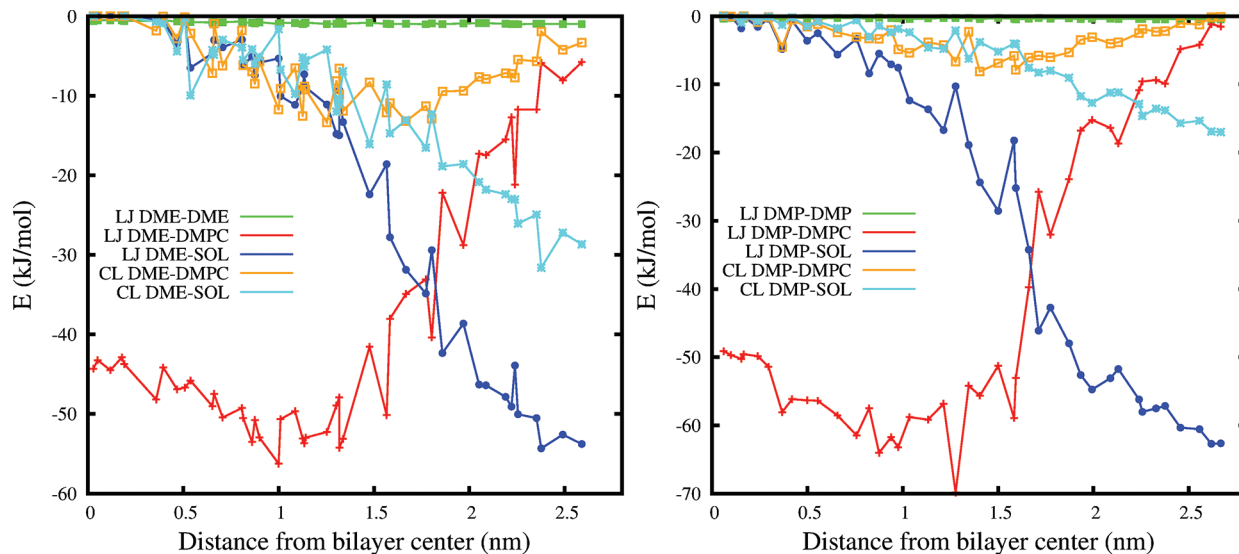


Figure 8. Nonbonded energy contributions calculated from all the frames of the US simulations: Lennard-Jones (LJ) and Coulombic (CL) energies for percolation of DME (left) and DMP (right) through DMPC.

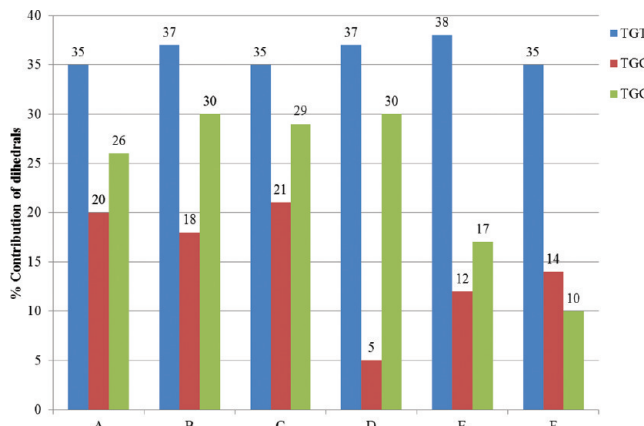


Figure 9. Comparison of the population distributions of the three dihedrals of the DME molecule for the six selected sets of simulations. The percentage of the most populated conformers, TGT, TGG' and TGG, are shown as blue, red and green bars, respectively. A–F denotes the selected sets (as shown in Figure 3).

variability also evidenced by the high fluctuations of the end-to-end distance of the molecule during the US simulation run (Figure S8a in the SI). This is also observed for simulation D, where the conformer fluctuates between the high and low dipole conformation, resulting in high fluctuation in the end-to-end distance. Interestingly, the end-to-end fluctuations for the DMP molecule are far less than the DME molecules (Figure S8 in the SI). This indicates a different entropic contribution to the overall free energy of percolation of the two molecules. The reduced mobility of the DMP molecule indicates minor disturbance in the ordered lipid tail region. In addition, it has been seen from the unconstrained simulations that the proximity of the polar region of the DMPC layer helps to stabilize the DMP molecule inside the bilayer. As a result, DMP tends to accumulate near the headgroup region once inside the bilayer (Figure 11). These factors result in the formation of a dip in the PMF profile of DMP in this region.

Considering the hydrogen bonding capability of the two molecules throughout the pathway, DME tends to form more

hydrogen bonds than DMP with an average number of 0.505 and 0.187 for DME and DMP, respectively (Figure S15 in the SI). However, once inside the bilayer, there is no chance of H-bonding in the aliphatic region of the bilayer. When compared to DMP, DME loses H-bonding to a larger extent, which causes greater loss of stability, resulting in higher PMF values.

To better understand the role of the electrostatic interaction on the percolation barrier, a set of US simulations of DME and DMP with the partial charges on all atoms set to zero were also performed. In Figure 10, the new calculated PMF profiles are compared with those of the charged models. For DME, the two PMF curves show large differences. On the contrary, that for the DMP molecule is similar and comparable to the uncharged DME one. These results indicate that partial charges and, hence, the associated dipoles of the two molecules play an important role in the percolation process of these molecules through the DMPC layer.

DME and DMP at water/DMPC interface. The estimated value of the barriers of permeation for DMP of ~ 12 kJ/mol is $\sim 4.65 kT$ (k = Boltzmann constant, $T = 310$ K), indicating a possible spontaneous insertion of DMP into the lipid bilayer. Therefore, unconstrained simulations for 50 ns were performed for both DME and DMP molecules for all six configurations shown in Figure 3. Density distributions of DME and DMP during the simulation along the Z-axis of the box for all the frames were calculated, and they are shown in Figure 11. The distribution indicates the affinity of DME toward the water phase. In all the simulations, the DME molecule moves away from the interior of the bilayer phase and accumulates close to the water interface, as evidenced by the large peaks at 5 nm. For the simulation started with the DME molecule in the center of the bilayer (frame F), the molecule resides in the polar headgroup region of the bilayer.

On the contrary, for DMP, all the simulations clearly show higher tendency of the molecule to reside in the aliphatic region of the bilayer (Figure 11). In all of the cases, except for simulation A, spontaneous diffusion of the DMP molecule into the bilayer is observed. In the case of simulation set A, for which in the starting conformation the DMP molecule was in the water phase away from the bilayer boundary, it does not

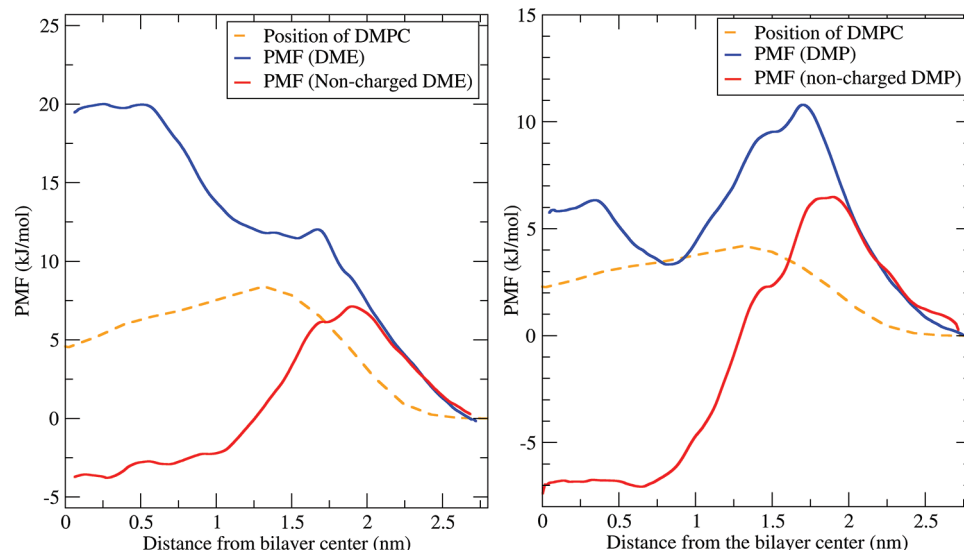


Figure 10. Comparison of the PMF profile for percolation of charged and noncharged DME (left) and DMP (right) in a DMPC layer obtained by the US method.

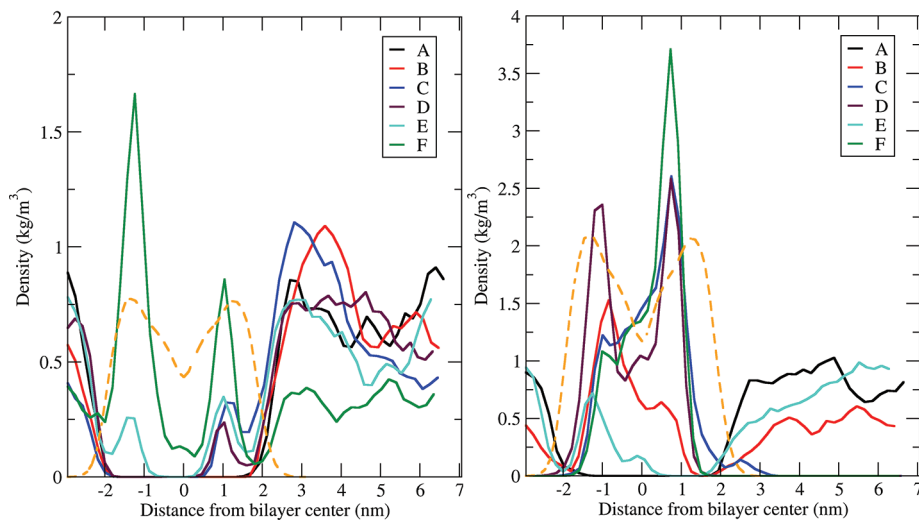


Figure 11. Average density distribution of DME (left) and DMP (right) during 50 ns of unconstrained simulation of the selected frames (Figure 3). The position of the DMPC bilayer is shown as an orange dashed line.

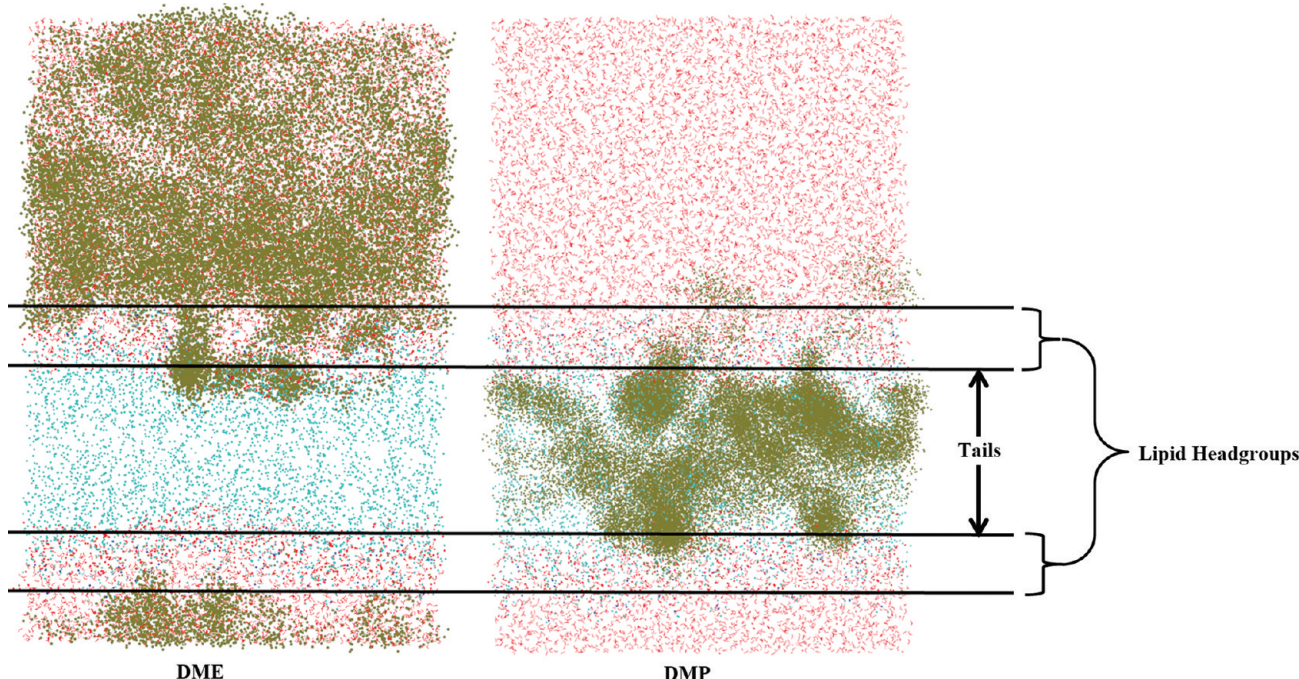


Figure 12. Probability distribution of DME (left) and DMP (right) in the system during a 50 ns simulation starting from a frame when the molecule is in the headgroup region (frame C from Figure 3). The position of the molecules at every 10 ps is shown as a gray dot.

diffuse inside the bilayer and tends to stay in the water phase. From the position of the maxima in the density distribution of DMP (for B–F simulation sets) in Figure 11, it is interesting to note that once inside the bilayer, the molecules slightly prefer to distribute close to the polar headgroup region. However, for simulation A, no specific preference of the DMP molecule for the polar headgroup is observed. Three sets of simulations for both DME and DMP were considered for further study. The starting positions of DME/DMP in these simulations are as follows:

- in the water phase 1 nm away from the bilayer boundary (frame A in Figure 3),
- in the headgroup region of the upper layer (frame C in Figure 3), and

(iii) in the aliphatic tail region of the bilayer near the bilayer center (frame F in Figure 3).

Simulations of DME and DMP starting from the water phase showed no spontaneous diffusion of the molecules into the bilayer for the simulation length (50 ns). The calculated diffusion coefficients from the CoM mean square displacement are equal to $0.7 \pm 0.01 \times 10^{-9} \text{ m}^2/\text{s}$ and $1.4 \pm 0.2 \times 10^{-9} \text{ m}^2/\text{s}$ for DME and DMP, respectively. From our previous work, the values of diffusion coefficients of DME and DMP models in pure water extrapolated at 310 K are $1.7 \times 10^{-9} \text{ m}^2/\text{s}$ and $1.4 \times 10^{-9} \text{ m}^2/\text{s}$, respectively.³⁷ Therefore, the diffusion coefficients of DME at the DMPC interface is significantly lower than that for bulk water. It has been known that at interfaces polyethylethers are slightly hydrophobic,⁵⁹ and their accumulation on the bilayer surface has been proven by X-ray

scattering studies.^{15,60} The free simulation indicates affinity of the DME molecules to the polar surface of lipid bilayer, resulting in very low diffusion coefficient values. DMP, having less affinity to the lipid bilayer surface (see Figure 11), has a higher diffusion coefficient, which is almost equivalent to that in pure water. In the second (ii) set of simulations, the distances and the number of contacts of the respective molecules from the DMPC chains were calculated and are shown in Figures 12 and 13 and Figure S12 in the SI. The value

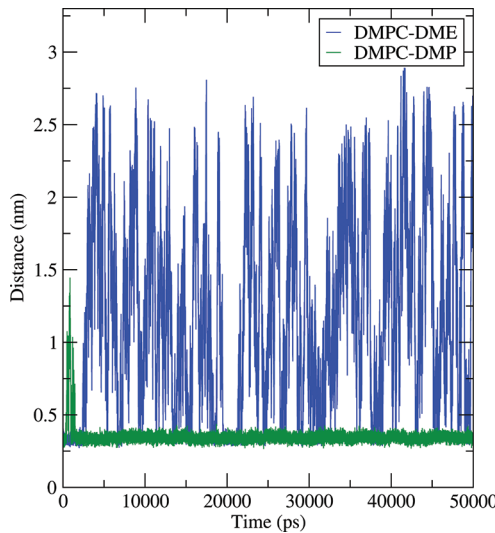


Figure 13. Distance of DME (blue) and DMP (green) from DMPC during a 50 ns simulation.

of distances clearly indicates that, during the simulation, the DMP molecule tends to stay in the tail region of the bilayer phase, whereas the DME molecule tends to move out of the lipid phase and stay in the water phase close to the bilayer (Figures 12 and 13). Calculating the average number of contacts for DME and DMP (within 0.6 nm of the DMPC lipid atoms) resulted in 14.6 and 163.1, respectively, which further supports this observation.

Finally, simulation (iii) shows a trend similar to that of the previous one. As expected from the calculated PMF profiles, the DMP molecule remains in the aliphatic region, whereas the DME molecule diffuses back to the water phase.

The calculated values of the diffusion coefficients for DME and DMP molecules in the lipid bilayer are $2.1 \pm 0.3 \times 10^{-9} \text{ m}^2/\text{s}$ and $0.6 \pm 0.1 \times 10^{-9} \text{ m}^2/\text{s}$, respectively. These values are also significantly lower than those in bulk *n*-heptane, which are $3.7 \times 10^{-9} \text{ m}^2/\text{s}$ for DME and $3.6 \times 10^{-9} \text{ m}^2/\text{s}$ for DMP, respectively.³⁷ The reduced diffusion coefficients with respect to the *n*-heptane is a consequence of the orderliness in the lipid tails that restricts free diffusion of the DMP molecule in the hydrophobic region. The larger effect on the DMP is a consequence of both the larger affinity with the hydrophobic part of the lipid tail and the larger steric hindrance due to the methyl group.

Simulations with Multiple DME and DMP Molecules at the Water/DMPC Interface. To understand the effect of the concentration of DME/DMP at the DMPC interface, two unconstrained simulations of 50 ns each were also run starting with nine DME and nine DMP molecules (approximately 0.6% molar fraction with respect to water), localized in the water phase $\sim 1 \text{ nm}$ away from the bilayer. The density distributions

of DME and DMP obtained from the simulations are compared in Figure 14. As for the single molecules, a similar trend is

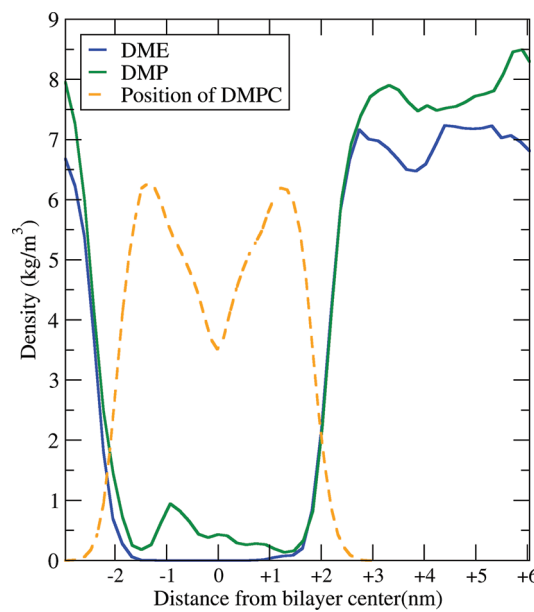


Figure 14. Average density distribution of nine molecules of DME and DMP during 50 ns of unconstrained simulation. The position of the DMPC bilayer is shown as an orange dashed line.

observed for DME. No spontaneous diffusion of DME inside the DMPC bilayer was observed. The maxima near the polar headgroup indicates the affinity of DME and DMP toward the polar headgroup of DMPC. In the case of DMP, positive density distribution inside the bilayer region indicates a spontaneous diffusion inside the membrane. From the visual inspection of the trajectory, one molecule of DMP was found to penetrate the lipid bilayer.

CONCLUSIONS

In this paper, structural, dynamic, and thermodynamic properties of DME and DMP in 1-octanol, water/*n*-heptane, and water/DMPC bilayer interfaces have been investigated with MD simulations. The Gibbs free energy of solvation of DME and DMP in 1-octanol and the partition coefficient values between water and 1-octanol show excellent agreement with available experimental data. This indicates that the models are suitable for use in complex environments such as lipid bilayer systems to study percolation behaviors.

The percolation properties of DME and DMP was first investigated at a water/*n*-heptane interface. The PMF curves for the percolation of both ethers from water to *n*-heptane to water phase were calculated. The calculated percolation barriers from water to the *n*-heptane phase were calculated equal to 18.5 and 5 kJ/mol for DME and DMP, respectively. It is shown that the better stabilization of DME in the water phase (in terms of Lennard-Jones as well as Coulombic potential) and relatively better stabilization of DMP (in terms of Lennard-Jones potential) in *n*-heptane causes the large differences in the two values.

The diffusion of DME and DMP through a DMPC bilayer was investigated. The PMF profile of bilayer percolation was obtained using the US method. The energy barrier to transfer the molecules from water into the DMPC tail region was calculated to be 20 and 12 kJ/mol for DME and DMP,

respectively. This height of the barrier in the tail region of DMPC is consistent with and comparable to that of the water/*n*-heptane system. The details of the percolation properties have been discussed based on nonbonded energy contributions and dynamic and structural properties of the molecules. This analysis showed extra stabilization for DME in correspondence to the headgroup region. This explains the accumulation of polyethers at the interface of the lipid bilayer as studied by Firestone et al. from X-ray scattering studies.^{15,60} It has also been shown that electrostatic interactions play an important role in the energetics of the bilayer percolation process for the DME molecule. Finally, the results of long unconstrained DME and DMP simulations further support the behavior expected from the PMF curves. If the simulations start with the molecules located in the lipid headgroup region, DMP molecules tend to spontaneously diffuse to the center of the lipid bilayer, while DME molecules prefer to remain in the lipid/water interface region. The spontaneous diffusion of DMP molecules to the interior of the lipid bilayer can be enhanced by increasing the concentration, as shown by simulations starting with multiple molecules in the water phase. On the contrary, no concentration effect has been observed for DME.

In conclusion, the results of this study provide interesting insights on the mechanism of percolation of DME and DMP ether molecules into a DMPC lipid bilayer. DME and DMP are the building blocks for larger di- and triblock amphiphilic copolymers (e.g., Pluronics), which are important and widely used for designing drug carrier micelles. Our results provide, for the first time, an accurate atomistic model on the partition behavior of hydrophilic (DME/PEO) and hydrophobic (DMP/PPO) blocks of these polymers at a membrane interface. Further computational studies are on the way to understand the effect of the polymer length and composition on the percolation process.

■ ASSOCIATED CONTENT

Supporting Information

Tables for conformer population and nonbonded energy contributions, figures of PMF profiles and plots obtained by SMD, detailed plots for nonbonded energy contributions for important sets of simulations, probability distribution of DME/DMP in the bilayer, and time evolution of area-per-lipid values are available in the Supporting Information. This material is available free of charge via the Internet at <http://pubs.acs.org>.

■ AUTHOR INFORMATION

Corresponding Author

*Address: Jacobs University Bremen, Campus Ring 1, D-28759, Bremen, Germany. Fax: +49 421 200-3249; Tel: +49 421 200-3144; E-mail: d.roccatano@jacobs-university.de.

Notes

The authors declare no competing financial interest.

■ ACKNOWLEDGMENTS

This project is funded by the Deutsche Forschungsgemeinschaft (DFG) for the project "The study of detailed mechanism of polymers/biological membrane interactions using computer simulation" (RO 3571/3-1).

■ REFERENCES

- (1) Forster, S.; Plantenberg, T. *Angew. Chem., Int. Ed.* **2002**, *41*, 689–714.
- (2) Fusco, S.; Borzacchiello, A.; Netti, P. A. *J. Bioact. Compat. Polym.* **2006**, *21*, 149–164.
- (3) Haag, R.; Kratz, F. *Angew. Chem., Int. Ed.* **2006**, *45*, 1198–1215.
- (4) Koder, Y.; Matsushima, A.; Hiroto, M.; Nishimura, H.; Ishii, A.; Ueno, T.; Inada, Y. *Prog. Polym. Sci.* **1998**, *23*, 1233–1271.
- (5) Alarcon, C. D. H.; Pennadam, S.; Alexander, C. *Chem. Soc. Rev.* **2005**, *34*, 276–285.
- (6) Chowdhary, R. K.; Sharif, I.; Chansarkar, N.; Dolphin, D.; Ratkay, L.; Delaney, S.; Meadows, H. *J. Pharm. Pharm. Sci.* **2003**, *6*, 198–204.
- (7) Schmolka, I. R. *Polymers for Controlled Drug Delivery*. In *Polymers for Controlled Drug Delivery*; Tarcha, P. J., Ed.; CRC Press: Boston, MA, 1991.
- (8) Oh, K. T.; Bronich, T. K.; Kabanov, A. V. *J. Controlled Release* **2004**, *94*, 411–422.
- (9) Sahu, A.; Kasoju, N.; Goswami, P.; Bora, U. *J. Biomater. Appl.* **2011**, *25*, 619–639.
- (10) Melik-Nubarov, N. S.; Pomaz, O. O.; Dorodnych, T. Y.; Badun, G. A.; Ksenofontov, A. L.; Schemchukova, O. B.; Arzhakov, S. A. *FEBS Lett.* **1999**, *446*, 194–198.
- (11) Otis, F. o.; Racine-Berthiaume, C.; Voyer, N. *J. Am. Chem. Soc.* **2011**, *133*, 6481–6483.
- (12) Gil, E. S.; Hudson, S. M. *Prog. Polym. Sci.* **2004**, *29*, 1173–1222.
- (13) Gabizon, A.; Shmeeda, H.; Barenholz, Y. *Clinical Pharmacokinetics* **2003**, *42*, 419–436.
- (14) Vonarbourg, A.; Passirani, C.; Saulnier, P.; Simard, P.; Leroux, J. C.; Benoit, J. P. *J. Biomed. Mater. Res., Part A* **2006**, *78*, 620–628.
- (15) Firestone, M. A.; Wolf, A. C.; Seifert, S. *Biomacromolecules* **2003**, *4*, 1539–1549.
- (16) Sevink, G. J. A.; Fraaije, J. G. E. M.; Huinink, H. P. *Macromolecules* **2002**, *35*, 1848–1859.
- (17) Lopez, C. F.; Nielsen, S. O.; Srinivas, G.; DeGrado, W. F.; Klein, M. L. *J. Chem. Theory Comput.* **2006**, *2*, 649–655.
- (18) Pal, S.; Milano, G.; Roccatano, D. *J. Phys. Chem. B* **2006**, *110*, 26170–26179.
- (19) Srinivas, G.; Klein, M. L. *Mol. Phys.* **2004**, *102*, 883–889.
- (20) Srinivas, G.; Shelley, J. C.; Nielsen, S. O.; Discher, D. E.; Klein, M. L. *J. Phys. Chem. B* **2004**, *108*, 8153–8160.
- (21) Hatakeyama, M.; Faller, R. *AIP Conf. Proc.* **2008**, *982*, 528–531.
- (22) Saiz, L.; Klein, M. L. *Acc. Chem. Res.* **2002**, *35*, 482–489.
- (23) Nielsen, S. O.; Lopez, C. F.; Srinivas, G.; Klein, M. L. *J. Phys.: Condens. Matter* **2004**, *16*, 481–512.
- (24) Isralewitz, B.; Gao, M.; Schulten, K. *Curr. Opin. Struct. Biol.* **2001**, *11*, 224–230.
- (25) Park, S.; Schulten, K. *J. Chem. Phys.* **2004**, *120*, 5946–5961.
- (26) Marrink, S.-J.; Berger, O.; Tieleman, P.; Jähnig, F. *Biophys. J.* **1998**, *74*, 931–943.
- (27) Stepaniants, S.; Izrailev, S.; Schulten, K. *J. Mol. Model.* **1997**, *3*, 473–475.
- (28) Jarzynski, C. *Phys. Rev. Lett.* **1997**, *78*, 2690–2693.
- (29) Park, S.; Khalili-Araghi, F.; Tajkhorshid, E.; Schulten, K. *J. Chem. Phys.* **2003**, *119*, 3559–3566.
- (30) Torrie, G. M.; Valleau, J. P. *J. Comput. Phys.* **1977**, *23*, 187.
- (31) Kumar, S.; Bouzida, D.; Swendsen, R. H.; Kollman, P. A.; Rosenberg, J. M. *J. Comput. Chem.* **1992**, *13*, 1011–1021.
- (32) MacCallum, J. L.; Bennett, W. F. D.; Tieleman, D. P. *Biophys. J.* **2008**, *94*, 3393–3404.
- (33) Orsi, M.; Sanderson, W. E.; Essex, J. W. *J. Phys. Chem. B* **2009**, *113*, 12019–12029.
- (34) Chew, C. F.; Guy, A.; Biggin, P. C. *Biophys. J.* **2008**, *95*, 5627–5636.
- (35) Orsi, M.; Essex, J. W. *Soft Matter* **2010**, *6*, 3797–3808.
- (36) Widge, A. S.; Matsuoka, Y.; Kurnikova, M. *Langmuir* **2007**, *23*, 10672–10681.
- (37) Hezaveh, S.; Samanta, S.; Milano, G.; Roccatano, D. *J. Chem. Phys.* **2011**, *135*, 164501–164511.

- (38) Berger, O.; Edholm, O.; Jahnig, F. *Biophys. J.* **1997**, *72*, 2002–2013.
- (39) Berendsen, H. J. C.; Postma, J. P. M.; van Gunsteren, W. F.; Hermans, J. Intermolecular Forces. In *Intermolecular Forces*; Pullman, B., Ed.; Reidel: Dordrecht, 1981; pp 331.
- (40) Jorgensen, W. L.; Madura, J. D.; Swenson, C. J. *J. Am. Chem. Soc.* **1984**, *106*, 6638–6646.
- (41) Garrido, N. M.; Queimada, A. J.; Jorge, M.; Macedo, E. A.; Economou, I. G. *J. Chem. Theory Comput.* **2009**, *5*, 2436–2446.
- (42) Hess, B.; Kutzner, C.; van der Spoel, D.; Lindahl, E. *J. Chem. Theory Comput.* **2008**, *4*, 435–447.
- (43) Humphrey, W.; Dalke, A.; Schulten, K. *J. Mol. Graphics* **1996**, *14*, 33–38.
- (44) Bussi, G.; Donadio, D.; Parrinello, M. *J. Chem. Phys.* **2007**, *126*, 14101–14107.
- (45) Berendsen, H. J. C.; Postma, J. P. M.; Vangunsteren, W. F.; Dinola, A.; Haak, J. R. *J. Chem. Phys.* **1984**, *81*, 3684–3690.
- (46) Hess, B.; Bekker, H.; Berendsen, H. J. C.; Fraaije, J. G. E. M. *J. Comput. Chem.* **1997**, *18*, 1463–1472.
- (47) Darden, T.; York, D.; Pedersen, L. *J. Chem. Phys.* **1993**, *98*, 10089–10092.
- (48) Kirkwood, J. *J. Chem. Phys.* **1935**, *3*, 300–313.
- (49) Villa, A.; Mark, A. E. *J. Comput. Chem.* **2002**, *23*, 548–553.
- (50) Delgado, E.; Jana, G. *Int. J. Mol. Sci.* **2009**, *10*, 1031–1044.
- (51) Wang, J.; Wang, W.; Huo, S.; Lee, M.; Kollman, P. A. *J. Phys. Chem. B* **2001**, *105*, 5055–5067.
- (52) Sangster, J. *Octanol–Water Partition Coefficients: Fundamentals and Physical Chemistry*; Wiley: Chichester, U.K./New York, 1997; pp 170.
- (53) CHEMICALLAND21. www.chemicaland21.com (accessed March 19, 2012).
- (54) Marrink, S. J.; Berendsen, H. J. C. *J. Phys. Chem.* **1996**, *100*, 16729–16738.
- (55) Bomqvist, B. R.; Warnheim, T.; Claesson, P. M. *Langmuir* **2005**, *21*, 6373–6384.
- (56) Noskov, B. A. *Colloid J.* **2006**, *68*, 588–596.
- (57) Sedev, R.; Exerowa, D.; Findenegg, G. H. *Colloid Polym. Sci.* **2000**, *278*, 119–123.
- (58) Sedev, R.; Steitz, R.; Findenegg, G. H. *Phys. B: Condensed Matter* **2002**, *315*, 267–272.
- (59) Israelachvili, J. *Proc. Natl. Acad. Sci. U.S.A.* **1997**, *94*, 8378–8379.
- (60) Firestone, M. A.; Seifert, S. *Biomacromolecules* **2005**, *6*, 2678–2687.